Computational modelling of cosmic rays in the neighbourhood of the Sun

M S Potgieter and R D Strauss

Centre for Space Research, North-West University, Potchefstroom, South Africa

E-mail: marius.potgieter@nwu.ac.za

Abstract. The heliosphere is defined as the plasmatic influence sphere of the Sun and stretches far beyond the solar system. Cosmic rays, as charged particles with energy between about 1 MeV and millions of GeV, arriving from our own Galaxy and beyond, penetrate the heliosphere and encounter the solar wind and embedded magnetic field so that when observed they contain useful information about the basic features of the heliosphere. In order to interpret these observations, obtained on and near the Earth and farther away by several space missions, and to gain understanding of the underlying physics, called heliophysics, we need to simulate the heliosphere and the acceleration, propagation and transport of these astroparticles with numerical models. These types of models vary from magnetohydrodynamic based approaches for simulating the heliosphere to using standard finite-difference numerical schemes to solve transport-type partial differential equations with varying complexity. A large number of these models have been developed locally to do internationally competitive research and have become as such an important training tool for human capacity development in computational physics in South Africa. How these models are applied to various aspects of heliospheric space physics, with illustrative examples, is discussed in this overview.

1. Introduction

The Sun has a plasmatic atmosphere that is blowing away from it at supersonic speeds between 450 km/s and 800 km/s and is called the solar wind. Embedded in this solar wind is a magnetic field and together they defined the influence sphere of the Sun which is called the heliosphere. Between 70-90 AU from the Sun, the solar wind becomes subsonic and creates a termination shock (TS); 1 AU is the averaged distance between the Earth and the Sun. At around 120 AU a heliopause (HP), is formed and much further out a bow shock. This whole region constitutes the heliosphere, as will be further illustrated and discussed in Figure 1, and can expand easily to 500 AU in the direction in which the heliosphere is moving through the local interstellar medium (ISM). The Sun has an 11-year activity cycle and on top of this, its magnetic field changes polarity every 11 years to create a 22-year cycle.

Cosmic rays are charged particles with energies from about 1 MeV up to EeV. The are accelerated to these energies in our Galaxy, and beyond, and penetrate the heliosphere from all directions. Below 50 GeV these particles are reduced systematically in the heliosphere, progressively more the lower the energy, to the point where this reduction becomes significant, typically below about 10 GeV. Since solar activity has an 11-year cycle, the cosmic ray flux is also modulated by this cycle, that is, as a function of time, space and energy. This is known as the solar modulation of cosmic rays.

There are four primary populations of charged particles in the heliosphere: Galactic cosmic rays entering the heliosphere from interstellar space while solar energetic particles are accelerated during so-called solar flare or coronal mass ejection events; then there is the anomalous cosmic ray component considered to be accelerated in the outermost regions of the heliosphere, and lastly, charged particles that originate from planetary magnetospheres, for example, from Jupiter and Saturn. See the review by [1].

Numerous space missions have contributed significantly over several decades to the observation of cosmic rays in the heliosphere, from the Earth to the HP. Presently, the two Voyager spacecraft explore the outer regions of the heliosphere, with Voyager 1 already beyond the HP [2] at a distance of 135 AU from the Sun.

2. Transport of cosmic rays in the heliosphere

The propagation of cosmic rays as charged particles in the heliosphere is generally described by a transport equation (TPE) derived by [3] as a special case of the general Fokker-Planck equation. Within a heliocentric spherical coordinate system, this equation can be expressed as

$$\underbrace{\frac{\partial f}{\partial t}}_{\text{a}} = -(\underbrace{\mathbf{V}_{sw}}_{\text{b}} + \underbrace{\langle \mathbf{v}_D \rangle}_{\text{c}}) \cdot \nabla f + \underbrace{\nabla \cdot (\mathbf{K}_s \cdot \nabla f)}_{\text{d}} + \underbrace{\frac{1}{3} (\nabla \cdot \mathbf{V}_{sw}) \frac{\partial f}{\partial \ln p}}_{\text{e}} + \underbrace{Q}_{\text{f}}, \tag{1}$$

for the omnidirectional distribution function $f(\mathbf{r}, p, t)$ of cosmic rays, where f is a function of position $\mathbf{r}$, particle momentum p and time t. The transport and modulation mechanisms contained in this equation are: (a) time-dependent changes in the cosmic rays, (b) outward convection caused by the expanding solar wind velocity $\mathbf{V}_{sw}$, (c) gradient, curvature and current sheet drifts in the global heliospheric magnetic field (HMF) in terms of the average drift velocity $\langle \mathbf{v}_D \rangle$, (d) spatial diffusion caused by the irregular HMF through the symmetric diffusion tensor $\mathbf{K}_s$, (e) adiabatic energy changes (deceleration or acceleration) determined by the solar wind divergence ($\nabla \cdot \mathbf{V}_{sw}$), and (f) possible additional sources of cosmic rays within the heliosphere, such as the Jovian and Cronian electrons. The diffusion tensor contains a diffusion coefficient parallel to the mean HMF, $\kappa_{||}$, and in two perpendicular directions, $\kappa_{\perp r}$ and $\kappa_{\perp \theta}$. All three depend on position, time and on the energy of the particles so that the underlying physics can be very complicated. This TPE has been applied to all the mentioned populations of cosmic rays; see [4] and [5] for overviews of these transport processes and cosmic ray modulation in general.

Solving this equation using different numerical techniques, while keeping the physics as up to date as possible, is the essence of the numerical modelling of cosmic rays in the heliosphere. A similar approach is used to solve the TPE for cosmic rays in the Galaxy although the transport and other processes, such as energy losses, can be different; see [6] and [7].

3. Modelling the heliosphere

Magnetohydrodynamic (MHD) models are frequently used to describe the main features of the heliosphere, for example, its full geometrical extent in all directions, and important issues such as where are the TS and the HP located. Most of these models are quite comprehensive and as such complicated, sometimes with overwhelming detail [10], or they can be designed to be of more practical use for cosmic ray studies as done by [9]. The latter serves the purpose of defining the basic features of the heliosphere as relevant to the study of cosmic ray modulation. As the Sun moves through interstellar space, the heliosphere interacts with the ISM so that the heliosphere is shaped into distinctive narrow nose and extended tail regions, where the narrower nose region points in the direction in which the heliosphere is moving.

In Figure 1, a MHD simulated meridional cut of the heliosphere is shown. The colour scales in the panels labelled (a) to (d) respectively indicate particle density, plasma speed, magnitude

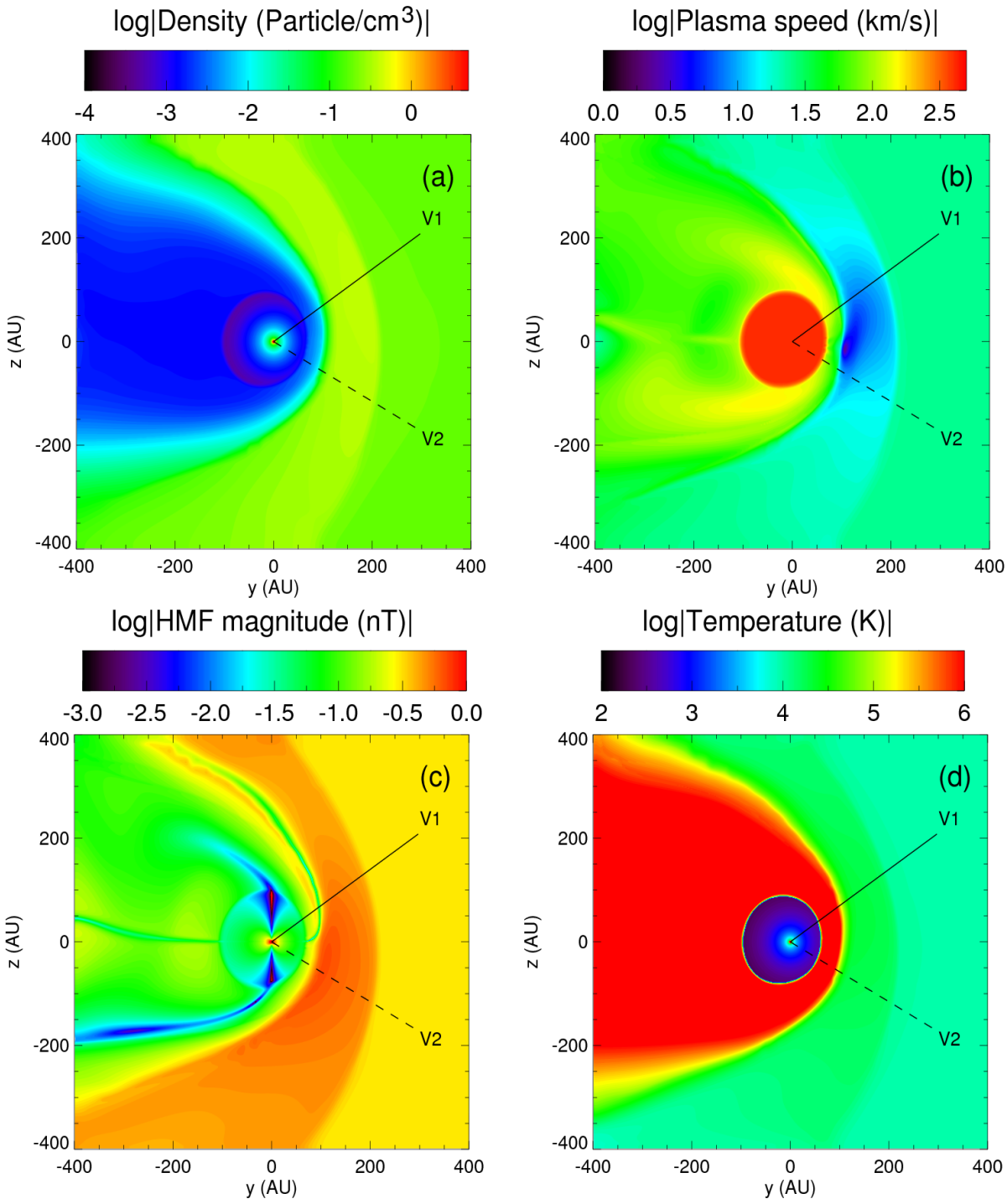

Figure 1. The MHD heliospheric environment in terms of particle density, plasma (solar wind) speed, magnitude of the heliospheric magnetic field, and temperature in the meridional plane as shown in panels labelled (a), (b), (c) and (d), respectively. This simulated heliosphere moves to the right through the interstellar medium. From right to left, notice the distinguishable structures in panel (c) particularly, first the bow shock, then the heliopause and termination shock, with the Sun at (0,0) AU. The approximate trajectories of the Voyager 1 and 2 spacecraft (projected onto the same plane) are indicated by the solid and dashed lines, respectively. Voyager 1 is now at about 135 AU, already beyond the heliopause, while Voyager 2 is at 112 AU. Figure is from [8], see also [9].

of the HMF and temperature. The ISM flow is from the right and the first notable structure to form is the bow shock (BS) at about 220 AU from the Sun in the nose direction along the solar equatorial plane. The assumed trajectories of the Voyager 1 and 2 spacecraft are also indicated, projected onto the same plane. According to this MHD approach, moving radially inward along the equatorial plane from the position of the BS, the HP is located at about 110 AU from the Sun. The HP separates the heliospheric medium from the ISM and as such serves as the effective boundary between the heliosphere and the local ISM. The region between the BS and the HP is known as the outer heliosheath. In this figure, at about 75 AU in the equatorial plane, the supersonic solar wind decreases to subsonic speeds so that the TS is formed. The region of the heliosphere between the HP and the TS is known as the inner heliosheath. The existence of the TS was confirmed when Voyager 1 and 2 crossed into the heliosheath at distances of 94 AU in 2004 and 84 AU in 2007, respectively. Voyager 1 crossed the HP at about 121 AU in August 2012, while Voyager 2 is still inside the inner heliosheath. (See also http://voyager.jpl.nasa.gov/).

A comprehensive approach to the numerical modelling of solar modulation consists of combining these MHD models with transport models for cosmic rays, the so-called hybrid models. For illustrative examples of such an approach and for several applications, see the recent modelling of [9] and [11].

4. Solar modulation models

The TPE in Eq. 1 written in terms of heliocentric spherical coordinates can be rearranged to emphasize the contributions of four major modulation processes which are: diffusion, particle drifts, convection and adiabatic energy losses, so that it becomes:

$$\begin{aligned}
&\overbrace{\left[\frac{1}{r^2}\frac{\partial}{\partial r}\left(r^2K_{rr}\right)+\frac{1}{r\sin\theta}\frac{\partial K_{\phi r}}{\partial\phi}\right]\frac{\partial f}{\partial r}+\left[\frac{1}{r^2\sin\theta}\frac{\partial}{\partial\theta}\left(K_{\theta\theta}\sin\theta\right)\right]\frac{\partial f}{\partial\theta}}^{\text{diffusion}} \\
+\;&\overbrace{\left[\frac{1}{r^2\sin\theta}\frac{\partial}{\partial r}(rK_{r\phi})+\frac{1}{r^2\sin^2\theta}\frac{\partial K_{\phi\phi}}{\partial\phi}-\Omega\right]\frac{\partial f}{\partial\phi}}^{\text{diffusion}} \\
+\;&\overbrace{K_{rr}\frac{\partial^2 f}{\partial r^2}+\frac{K_{\theta\theta}}{r^2}\frac{\partial^2 f}{\partial\theta^2}+\frac{K_{\phi\phi}}{r^2\sin^2\theta}\frac{\partial^2 f}{\partial\phi^2}+\frac{2K_{r\phi}}{r\sin\theta}\frac{\partial^2 f}{\partial r\partial\phi}}^{\text{diffusion}} \\
+\;&\overbrace{\left[-\langle\mathbf{v}_D\rangle_r\right]\frac{\partial f}{\partial r}+\left[-\frac{1}{r}\langle\mathbf{v}_D\rangle_\theta\right]\frac{\partial f}{\partial\theta}+\left[-\frac{1}{r\sin\theta}\langle\mathbf{v}_D\rangle_\phi\right]\frac{\partial f}{\partial\phi}}^{\text{drift}} \\
-\;&\overbrace{V_{sw}\frac{\partial f}{\partial r}}^{\text{convection}}+\overbrace{\frac{1}{3r^2}\frac{\partial}{\partial r}\left(r^2V_{sw}\right)\frac{\partial f}{\partial\ln p}}^{\text{adiabatic energy losses}}=0,
\end{aligned} \tag{2}$$

given here in terms of five different diffusion coefficients; Ω is the rotational speed of the Sun.

In order to solve this TPE it is written in a condensed form, in terms of P, the particle's rigidity (momentum/charge), as

$$\begin{aligned}
&a_0(r,\theta,\phi,P)\frac{\partial f}{\partial r}+b_0(r,\theta,\phi,P)\frac{\partial f}{\partial\theta}+c_0(r,\theta,\phi,P)\frac{\partial f}{\partial\phi}+d_0(r,\theta,\phi,P)\frac{\partial^2 f}{\partial r\partial\phi} \\
+\;&e_0(r,\theta,\phi,P)\frac{\partial^2 f}{\partial r^2}+l_0(r,\theta,\phi,P)\frac{\partial^2 f}{\partial\theta^2}+m_0(r,\theta,\phi,P)\frac{\partial^2 f}{\partial\phi^2} \\
+\;&s_0(r,\theta,\phi,P)\frac{\partial f}{\partial\ln P}=0.
\end{aligned} \tag{3}$$

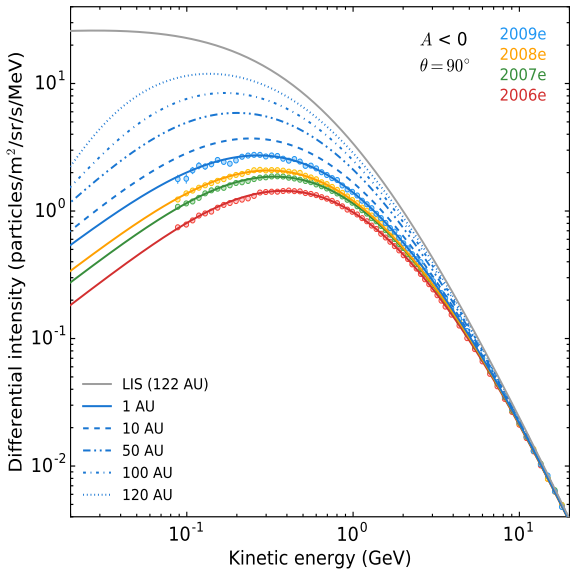

Figure 2. Computed proton spectra as a function of kinetic energy at the Earth (1 AU) are shown in comparison with observed spectra from the PAMELA space detector for the periods 2006e, 2007e, 2008e and 2009e. Additional computed spectra are shown in the heliospheric equatorial plane ($\theta = 90°$) at 10 AU, 50 AU, 100 AU and 120 AU (blue lines) with respect to a new very local interstellar spectrum (LIS; solid grey line) from [14] and [15], specified at 122 AU, assumed to be the position of the HP.

This is a parabolic differential equation which can be solved with a modified Crank-Nicholson finite difference method, called the Alternating Direction Implicit (ADI) method. For cosmic ray studies, this ADI method, as described by [12], is modified to include three spatial coordinates and energy (rigidity). Adding a fifth numerical dimension does not work well when using this ADI approach so that when time-dependent modulation is simulated, one of the spatial dimensions, typically the ϕ-dependence, is substituted by a time-dimension.

The very local interstellar spectra (LIS) of various cosmic ray species (from hydrogen to iron, including electrons, positrons and anti-particles) are taken as individual input spectrum at the outer boundary of the heliosphere, which typically is considered to be the HP for all values of θ and ϕ, while the inner boundary is taken close to the solar surface. At the heliospheric poles ($\theta = 0; \pi$), it usually is assumed that $\partial f/\partial\theta = 0$, so that a symmetry exists with respect to the heliospheric polar line, mostly done to same computational time.

For the ADI approach, an initial solution is obtained at one third of a rigidity step forward by solving Eq. 3 implicitly in the direction of the first spatial coordinate, i.e. radial distance r. A second solution is then calculated at another third of a rigidity step forward, using the first solution, by solving the differential equation implicitly in the direction of the second spatial coordinate, the polar angle θ. For a solution at the final third of the rigidity step, this process is repeated for the last spatial coordinate, the azimuthal angle ϕ, using the previous two solutions. As a result, a system of linear equations is obtained which can be solved using, for example, the Thomas algorithm. In the process, a 3D grid is constructed across which the TPE is solved. The radial grid points $r_i = (i-1)\Delta r + r_1$, for $i = 1, 2, \ldots, N_r$, run from $r = r_1$ at the inner boundary to $r = r_b$ at the outer boundary, with the radial increments $\Delta r = (r_b - r_1)/(N_r - 1)$. The polar grid points are $\theta_j = (j-1)\Delta\theta$, for $j = 1, 2, \ldots, N_\theta$, and run from $\theta = 0°$ at the north pole to $\theta = 180°$ at the south pole, with increments of $\Delta\theta = \pi/(N_\theta - 1)$. The azimuthal

grid points $\phi_k = (k-1)\Delta\phi$, for $k = 1, 2, \ldots, N_\phi$, run from $\phi = 0°$ to $\phi = 360°$ for a full solar rotation, where the azimuthal increments are $\Delta\phi = 2\pi/(N_\phi - 1)$. Furthermore, the rigidity decreases logarithmically from an initial maximum value P_{max} to a minimum value P_{min}, so that $P_{n+1} = P_n/\exp(\Delta \ln P)$, for $n = 1, 2, \ldots$, with $\Delta \ln P > 0$ the rigidity increment. The solution, however, becomes unstable when the rigidity steps are large relative to the squares of the spatial increments, so that the value for $\Delta \ln P$ is chosen mostly in order to improve the stability of the solution.

In terms of the generalized grid points, the distribution function is

$$f(r_i, \theta_j, \phi_k, P_n) = f(i\Delta r, j\Delta\theta, k\Delta\phi, n\Delta \ln P) = f_{i,j,k,n}, \tag{4}$$

so that, from Taylor series expansions, standard central finite difference approximations for the first, second and mixed derivatives of f are obtained. The solutions for f at the different rigidity steps are indicated by

$$f_{i,j,k,n} = f_{i,j,k}; f_{i,j,k,n+\frac{1}{3}} = f^*_{i,j,k}; f_{i,j,k,n+\frac{2}{3}} = g_{i,j,k}; f_{i,j,k,n+1} = h_{i,j,k}; \tag{5}$$

where for the first solution, $f^*_{i,j,k}$, is calculated by solving Eq. 3 implicitly in the radial direction at one third of a rigidity step backward. This is achieved by evaluating half of the central difference equations in r at the current rigidity step and half of them at a third of a rigidity step backward. For the second solution, $g_{i,j,k}$, this process is repeated by once again solving Eq. (3) implicitly, in terms of $f^*_{i,j,k}$, in the θ-direction. Similarly, the third solution, $h_{i,j,k}$, in terms of $f^*_{i,j,k}$ and $g_{i,j,k}$, is obtained at one full rigidity step backward by solving Eq. 3 implicitly in the ϕ-direction. This process is repeated for all rigidity values in order to obtain a solution for the final distribution function f, which is related to the differential intensity $j = P^2 f$.

A typical solution of Eq. 2 is shown in Figure 2. It depicts computed proton spectra in the solar equatorial plane ($\theta = 90°$) at 1 AU, 10 AU, 50 AU, 100 AU and 120 AU, relative to the LIS for protons, specified at the HP located here at 122 AU [14]. Four computed spectra are compared to the observed proton spectra from the PAMELA space experiment (http://pamela.roma2.infn.it/index.php) for November 2006, December 2007, December 2008 and December 2009, indicated as 2006e, 2007e, 2008e and 2009e [14]. This shows that these types of numerical models are successful at reproducing major cosmic ray observations. For more elaborate computations of radial and latitudinal gradients for cosmic rays throughout the heliosphere, see [13] and [15].

5. SDE models

The calculus of stochastic differential equations (SDEs) is a well developed field and the reader is referred to the work of [16] and [17] in which the relevant references are given.

For the purpose of this overview, it suffices to define an SDE as one that can be cast into the general form

$$\frac{\partial x(t)}{\partial t} = \mu(x,t) + \sigma(x,t)\zeta(t), \tag{6}$$

for a one-dimensional (1D) case where $\mu(x,t)$ and $\sigma(x,t)$ are continuous functions, while $\zeta(t)$ represents a rapidly varying stochastic function, also referred to as the noise term. The first and second terms on the right hand side of this equation are referred to as the drift and diffusion terms, respectively, and should not to be confused with the physical drift and diffusive terms present in the TPE. Moreover, only SDEs of the Itō type are considered, so that this equation can be rewritten as

$$dx(t) = \mu(x,t)dt + \sigma(x,t)dW(t), \tag{7}$$

where $dW(t)$ represents the Wiener process. This is a time stationary stochastic Levy process where the time increments have a Normal distribution with a mean of zero (i.e. a Gaussian

distribution) and a variance of dt; $dW(t) = W(t) - W(t - dt) \sim \mathcal{N}(0, dt)$. Eq. (7) can be integrated as

$$x(t) = x_0 + \int_0^t \mu(x, t^{'})dt^{'} + \int_0^t \sigma(x, t^{'})dW(t^{'}), \tag{8}$$

where the first integral is a normal (Riemann or Lebesgue) integral, while the second is an Itō type stochastic integral. Since analytical solutions for SDEs are only available for a limited few scenarios, this equation is usually integrated numerically, using the Euler-Maruyama numerical scheme [18], where a finite time step Δt is chosen so that

$$x^{t+\Delta t} = x^t + \mu(x, t)\Delta t + \sigma(x, t)\Delta W(\Delta t), \tag{9}$$

from an initial position $x = x_0$ at time $t = 0$ and continued until the boundary is reached at $x = x_\mathrm{e}$ at $t = t_\mathrm{e}$, or until a temporal integration limit is reached at $t = t^\mathrm{N}$. The Wiener process is discretized as

$$\Delta W(\Delta t) = \sqrt{\Delta t} \cdot \Lambda(t), \tag{10}$$

where $\Lambda(t)$ is a simulated Gaussian distributed pseudo-random number, which should be handled with great care. The temporal evolution of x forms a trajectory through phase space, which is generally referred to as the trajectory of a pseudo-particle. Integrating Eq. 8 for a single pseudo-particle has limited significance so that integration is carried out over all possible trajectories, usually done $N \gg 1$ times; this is also referred to as tracing N pseudo-particles.

A normalised (conditional) probability density $\rho^{'}(x, t)$ can be calculated from the pseudo-particle trajectories, such that

$$\int_\Omega \rho^{'}(x, t)d\Omega = 1, \tag{11}$$

where Ω denotes the entire integration space. Numerically this is done by dividing e.g. x into a series of bins, e.g. $N^{'}$ intervals, and calculating the number of pseudo-particles ending up in each bin, i.e. bin i has N_i particles, and dividing by N. The discretized version of this equation thus reads

$$\sum_{i=1}^{N^{'}} \rho_i^{'}(x, t) = \sum_{i=1}^{N^{'}} \frac{N_i}{N} = 1. \tag{12}$$

The set of SDEs for cosmic ray transport in heliocentric spherical dimensions (r,θ,ϕ) and momentum (p) is

$$\begin{array}{lcl} dr & = & \mu_r \cdot ds + \sigma_{rr} \cdot dW_r + \sigma_{r\theta} \cdot dW_\theta + \sigma_{r\phi} \cdot dW_\phi \\ d\theta & = & \mu_\theta \cdot ds + \sigma_{\theta\theta} \cdot dW_\theta + \sigma_{\theta\phi} \cdot dW_\phi \\ d\phi & = & \mu_\phi \cdot ds + \sigma_{\phi\phi} \cdot dW_\phi \\ dp & = & \mu_p \cdot ds, \end{array} \tag{13}$$

which can be integrated as mentioned above. The coefficients σ_{ij} are related to the elements of tensor in the TPE as in Eq. 1, with specifics as given in Eq. 2. The full set of SDEs to solve for the 3D transport of cosmic rays in the heliosphere is given in detail by [8] and [19]; see also [17] .

The momentum SDE can be rewritten in terms of the kinetic energy of particles as

$$dE = 1/3\,(\nabla \cdot \mathbf{V}_{sw})\,\Gamma E \cdot ds, \tag{14}$$

with

$$\Gamma \equiv (E + 2E_0)/(E + E_0), \tag{15}$$

where E_0 is the rest mass energy.

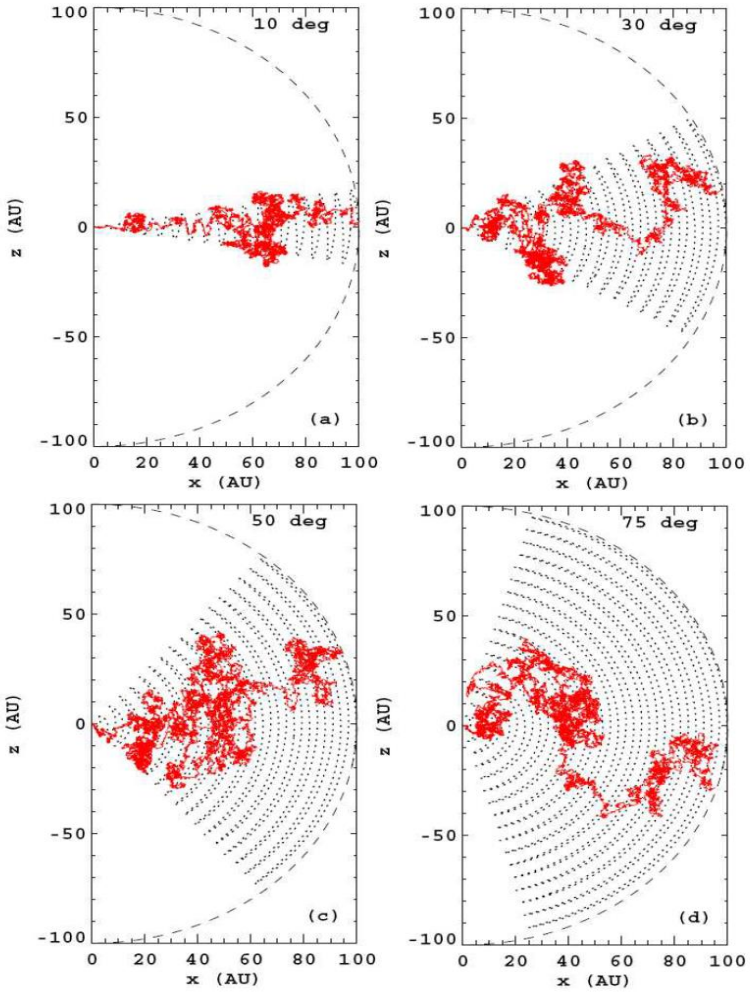

Figure 3. Pseudo-particle trajectories (red stochastic-like lines) for 100 MeV galactic protons propagating through the heliosphere towards the Earth at 1 AU, projected onto the meridional plane with the Sun at (0,0) AU. The HP position, in this example at 100 AU, is indicated by the circular dashed line, while the dotted line shows a projection of the wavy heliospheric current sheet onto the same plane, for four values of its tilt angle, shown as the dotted background lines. This figure is from [21].

This TPE usually is solved by means of SDEs in a so-called time-backward fashion. The time-forward and time-backward approaches are equivalent, but for cosmic ray modulation the latter approach is numerically more optimal and computationally much faster, with an appropriate handling of outer and inner boundary conditions. The use of SDE-models to solve the TPE, in order to overcome the characteristic problems and issues associated with finite-difference and finite-volume numerical schemes in higher dimensions, has been quite successful.

The validity and reliability of the SDE-based numerical model have been established in the past by extensive benchmarking. In the benchmarking and applications of [16], [20] and [21], the SDE-based model was utilised to model various aspects of the modulation of cosmic rays in the simulated heliosphere, serving as confirmation that the SDE approach is indeed reproducing the

basic features of cosmic ray modulation. The SDE-based models also allow for the calculation of pseudo-particle trajectories, from which valuable insight into the solar modulation process is gained.

Pseudo-particle trajectories are shown in Figure 3 for galactic protons with kinetic energy of 100 MeV. Four different scenarios of the wavy heliospheric current sheet (HCS) are shown, indicated by different tilt angles, from a small value of 10 degrees (top, left panel) to a large value of 75 degrees (bottom right panel). The latter represents maximum solar activity and the former solar minimum activity when maximum cosmic ray intensity occur, as was observed in 2009 (see Figure 2). The dashed line shows the position of the HP, whereas the dotted line shows a projection of the wavy HCS onto the meridional plane. These traces are indicative of how cosmic ray protons propagate into the heliosphere through the equatorial regions, following the HCS to a large extent while its waviness is small but they get significantly scattered off the HCS with increasing solar activity, as the tilt angle increases. Evidently, under these conditions these particles propagate mainly in latitudes covered by this HCS; see [21] for further elaborations.

It is worthwhile to mention that negatively charged cosmic rays, such as galactic electrons or anti-protons, will propagate differently into the heliosphere depending on the polarity of the HMF. This creates what is known as charge-sign dependent modulation which is an important special feature in the 22-year cycles of the solar modulation of cosmic rays; see the review by [5].

6. Implementing GPUs

The computing power of graphics processing units (GPUs) has become readily accessible with the introduction of Nvidia's CUDA (Compute Unified Device Architecture) parallel computing platform and application programming interface (API) almost ten years ago. The primary advantage of utilizing the massive parallel design of the CUDA architecture, is the significant increase in runtime performance compared to central processing units (CPUs). Many fields of science have benefited from the gain in performance that GPUs and the CUDA API can offer, including space and heliospheric physics.

A GPU-based modulation model for which the CUDA API was used to solve the TPE given above and to simulate the transport of charged particles using SDEs was introduced by [22]. A comparison was made between the run-times of the GPU-based model and a CPU version of the same model. The latter model was also optimized with OpenMP (Open Multi-Processing), a multi-thread technique that facilitates parallel processing in CPUs. Because SDE modulation models calculate the trajectory of individual pseudo-particles, where the computation of each trajectory is independent of all other trajectories, the process can easily be done in parallel. This GPU-based model [22] showed a performance increase of a factor of between ~ 10 and ~ 60 over the usual CPU-model, depending on the choice of input parameters.

The modulation model based on a finite difference numerical scheme as described above give a solution at each rigidity-step which depends on the solution from the previous rigidity-step, which makes these type of numerical models not fully parallelizable. However, numerous variables and modulation parameters, such as the solar wind speed, HMF-values and the diffusion coefficients, have to be calculated at each of the grid points in the simulated heliosphere. Such calculations across large arrays are parallelizable and can be performed much faster by using the CUDA API as opposed to performing the calculations sequentially with a CPU, or even with CPU-based parallel systems like OpenMP or MPI (Message Passing Interface). This advantage that CUDA offers has been exploited in order to perform all of the time-expensive array-based calculations, resulting in a runtime performance increase of a factor of between ~ 10 and ~ 20. Even though CUDA is capable of achieving significant performance increases for calculations that can be performed independently, the application of this technology to traditional finite difference numerical schemes remains a challenge. The best approach for improving runtime performance

in such models will be to use a combination of CPU and GPU computing resources; see [13] for details. For scaling and efficiency factors done for the SDE and CUDA approaches, see [22] and [23].

7. Summary

State-of-the-art numerical models have been developed over the years in the Centre for Space Research at the North-West University in South Africa. Because of the substantial computational skills required to develop these models, the process has become a good and productive training school for computational physics in South Africa.

The application of the described ADI-based models has made a significant impact on the study of the solar modulation of cosmic rays in the heliosphere as comprehensively reviewed by [4].

The SDE approach has proven to be remarkably successful in describing the heliospheric modulation of these particles. Numerically, SDE-based models are relatively easier to construct than a 3D finite difference model, and being unconditionally stable, makes it possible to study cosmic ray transport phenomena for a broader range of scenarios, while utilizing the power of modern day parallel computers. The CUDA version of the code is considerably faster than a multi-threaded CPU implementation and even small clusters. The GPU-approach can be of benefit when using modern desktop computers or if large CPU clusters are not accessible.

Acknowledgments

The authors thank Andreas Kopp, Xi Lou, Etienne Vos and Jan-Louis Raath for valuable discussions, and thank the South African National Research Foundation (NRF) for providing partial research funding and the Centre for High Performance Computing (CHPC) in Cape Town for allocating computational time.

References

[1] Strauss R D, Potgieter M S and Ferreira S E S 2012 *Adv. Space Res.* **49**, 392
[2] Gurnett D A, Kurth W S, Burlaga L F and Ness N F 2013 *Science* **341** 1489
[3] Parker E N 1965 *Planet. Space Sci.* **13** 9
[4] Potgieter M S 2013 *Living Rev. Solar Phys.* **10** 3
[5] Potgieter M S 2014 *Adv. Space Res.* **53** 1415
[6] Strong A W and Moskalenko I V 1998 *Astrophys. J.* **509** 212
[7] Kopp A, Büsching I, Potgieter M S, Strauss R D 2014 *New Astron.* **30** 32
[8] Strauss R D 2013 PhD thesis (North-West University, Potchefstroom, South Africa)
[9] Strauss R D, Potgieter M S, Ferreira S E S, Fichtner H and Scherer K 2013 *Astrophys. J. Lett.* **765** L18
[10] Opher M, Drake J F, Zieger B and Gombosi T I 2015 *Astrophys. J.* **800** L28
[11] Luo X, Zhang M, Potgieter M S, Feng X and Pogorelov P 2015 *Astrophys. J.* **808** 82
[12] Douglas J 1962 *Numerische Mathematik* **4** 41
[13] Vos E E 2016 PhD thesis (North-West University, Potchefstroom, South Africa)
[14] Vos E E and Potgieter M S 2015 *Astrophys. J.* **815** 119
[15] Vos E E and Potgieter M S 2016 *Solar Phys.* in press
[16] Strauss R D, Potgieter M S, Büsching I and Kopp A 2011a *Astrophys. J.* **735** 83
[17] Kopp A, Büsching I, Strauss R D and Potgieter M S 2012 *Comp. Phys. Comm.* **183** 530
[18] Maruyama G. 1955 *Rend. Circ. Mat. Palermo* **4** 48
[19] Raath J L, Potgieter M S, Strauss R D and Kopp A 2016 *Adv. Space Res.* **57** 1965
[20] Strauss R D, Potgieter M S, Kopp A and Büsching I 2011b *J. Geophys. Res.* **116** 105
[21] Strauss R D, Potgieter M S, Büsching I and Kopp A 2012 *Astrophys. Space Sci.* **339** 223
[22] Dunzlaff P, Strauss R D and Potgieter M S 2015 *Comp. Phys. Comm.* **192** 156
[23] Strauss R D and Moeketsi D M 2016 *Proc. Conf. South Afr. Inst. Phys.* in press